IEEE Access
Multidisciplinary | Rapid Review | Open Access Journal

Received July 12, 2019, accepted July 23, 2019, date of publication July 26, 2019, date of current version August 13, 2019.

Digital Object Identifier 10.1109/ACCESS.2019.2931344

Grid-Based Exclusive Region Design for 3D UAV Networks: A Stochastic Geometry Approach

KEIJI YOSHIKAWA, (Student Member, IEEE), KOJI YAMAMOTO, (Member, IEEE), TAKAYUKI NISHIO, (Member, IEEE), AND MASAHIRO MORIKURA, (Member, IEEE)
Graduate School of Informatics, Kyoto University, Kyoto 606-8501, Japan

Corresponding author: Koji Yamamoto (kyamamot@i.kyoto-u.ac.jp)

This work was supported by the research contract, Research and Development on Control Schemes for Utilization of Multiple Mobile Communication Networks, of the Ministry of Internal Affairs and Communications, Japan.

ABSTRACT This paper presents a stochastic geometry analysis of radio interference and a grid-based design of a primary exclusive region (PER) for spectrum sharing in the 3D unmanned aerial vehicle (UAV) networks. When a UAV network shares frequency bands with a primary system (e.g., a weather radar system), the UAVs must avoid harmful interference with the primary system. To facilitate the design of a complex-shaped PER according to a primary user's antenna pattern, spatial grid models, namely cylindrical and cubic grid models, are introduced. In the cylindrical grid model, to approximate the distribution of the interference at the radar, the cumulants of the interference are expressed by expressions with simple integrals or even closed-form expressions based on the assumption that the distributions of the UAVs in each grid cell follow an inhomogeneous 3D Poisson point process (PPP). In the cubic grid model, the shape of the grid cell is approximated by the cylindrical grid cell to derive the cumulants of the interference because they cannot be calculated in the same manner as in the cylindrical grid model. Using the derived interference cumulants to determine a PER to satisfy the radar's outage probability target, an optimization problem that minimizes the number of the UAVs forbidden from transmitting signals is formulated. The numerical results confirm that the approximated interference distribution using cumulants is in acceptable agreement with the simulation results and the PER obtained from the proposed optimization problem improves the number of the transmitting UAVs by reducing the volume of grid cells.

INDEX TERMS Cognitive radio, spectrum sharing, unmanned aerial vehicle (UAV), spatial grid, stochastic geometry, wireless communication.

I. INTRODUCTION

Spectrum sharing is an important issue in unmanned aerial vehicle (UAV) networks. The usage of UAVs is increasing and their communications require large capacity and high speed for their wide range of application. To fulfill the aforementioned requirements, in addition to narrow dedicated bands, wide shared bands (e.g., 5.7 GHz band) are proposed for UAV transmissions [1]. However, primary users exist in these wide shared bands, and thus UAV communications are secondary and must avoid harmful interference to the primary users.

We investigate a grid-based primary exclusive region (PER) for spectrum sharing. The PER was introduced in [2] for cognitive networks. The secondary users inside the PER are forbidden from transmitting to guarantee a desired performance for the primary user. In [3], the authors proposed a PER update framework that determines the optimal PER radius to minimize the area of the PER or maximize the transmission capacity of the secondary network. Given the primary user's receiver antenna patterns and the secondary user's transmitters density and transmission power, a spatial grid-based PER is introduced in [4]. The authors divide the two-dimensional (2D) space into polar grids or square grids to design a complex-shaped PER. With respect to UAV networks, the 3D space should be treated to consider the height. The authors in [5] extended the standard concept of planar 2D cellular networks into 3D space. In [6], the authors examined the concept of spectrum sharing of UAV small cell networks. They indicated that a 3D PER is determined as an upper-hemisphere or upper-hemisphere segment based on the radius of the PER and the height limit. In [7], the authors proposed the use of a cumulant matching approach to optimize the

The associate editor coordinating the review of this manuscript and approving it for publication was Jose Saldana.

radius of an upper-hemisphere PER in 3D UAV networks. However, it is necessary to design a practical PER based on the primary user's antenna pattern to maximize the number of transmitting UAVs. For example, [8] designed a PER based on a cylindrical grid model using stochastic geometry analysis of the interference.

Stochastic geometry is a powerful mathematical tool that is used to analyze the performance metrics of wireless networks that exhibit random topologies [9], [10]. Several studies have examined spectrum sharing using stochastic geometry. In [11], the authors analyzed device-to-device spectrum sharing by modeling the positions of the nodes as a random spatial Poisson point process (PPP). PPP is typically used to model the distribution of wireless nodes owing to its tractability [10]. In [3], the authors analyzed the aggregate interference at a primary user's receiver with a probability generating functional (PGFL) for the PPP.

This study presents a stochastic geometry analysis of the interference in UAV networks and proposes the design of a grid-based 3D PER. To design the PER according to a primary user's antenna pattern, a 3D space is divided into cylindrical and cubic grid cells. In the cylindrical grid model, to determine the distribution of the interference at the radar, the cumulants of the interference are expressed by expressions with simple integrals based on the assumption that the distributions of the UAVs in each grid cell follow an inhomogeneous 3D PPP. Furthermore, we expand the square grid model used in 2D systems [12], [13] to the cubic grid model in 3D UAV networks. In the cubic grid model, we approximate the shape of the grid cell by the cylindrical grid cell to derive the cumulants of the interference because they cannot be calculated in the same manner in the cylindrical grid model. Using the derived interference cumulants, we analytically derive the radar's outage probability (OP), which is defined as the probability that the aggregated interference power at the primary user from the UAVs exceeds a threshold. Subsequently, the UAV's allowable transmission probability (ATP) is introduced in each grid cell to design a complex-shaped PER. Moreover, we formulate an optimization problem that minimizes the number of UAVs forbidden from transmitting under the OP target for the primary user.

The contributions of this paper are twofold. The first contribution corresponds to the analysis of the OP at the primary user in 3D networks based on the spatial grid models using stochastic geometry. Specifically, the approximation for the cubic grid cells allows the expression of the cumulants of the interference as simple integral expressions or even as closed-form expressions. The second contribution is the design of the optimization framework for a 3D-shaped PER based on the derived interference cumulants, which increases the number of UAVs who can transmit without causing harmful interference to the primary user.

This paper is organized as follows. Section II presents the system model based on the spatial grid model. Section III derives the interference cumulants and the radar's OP using stochastic geometry. Section IV formulates the optimization problem to design the complex-shaped PER. Section V explains the numerical evaluation. Finally, the conclusions are presented in Section VI.

TABLE 1. Notation.

M_r	Number of radial divisions (cylindrical grid)
M_θ	Number of angular divisions (cylindrical grid)
M_z	Number of height divisions (cylindrical grid)
U_{ijk}	Grid cell (cylindrical grid)
R	Radius of U_{0jk} (cylindrical grid)
L	Height of each sector (cylindrical grid)
N_x	Number of x-axis divisions (cubic grid)
N_y	Number of y-axis divisions (cubic grid)
N_z	Number of z-axis divisions (cubic grid)
V_{ijk}	Grid cell (cubic grid)
ℓ	Length of side of cube (cubic grid)
$\lvert\cdot\rvert$	Volume (Lebesgue measure)
S	Grid cell, $S = U_{ijk}$ or $S = V_{ijk}$
λ_S	Density of UAVs for S
g_S	Antenna gain of radar for S
Φ_S	Locations of UAVs in S following inhomogeneous 3D PPP
Λ_S	Intensity function of PPP for S
a_S	UAV's allowable transmission probability in S
$\hat{\Phi}_S$	Locations of UAVs in S after applying ATP
I_{total}	Aggregated interference power at radar
I_{th}	Threshold in interference
I_S	Interference at radar from S
h_d	Fading gain between d and origin
p_S	Transmission power of UAVs in S
$\lVert\cdot\rVert$	Euclidean distance
α	Path-loss exponent
$\kappa_n(\cdot)$	nth cumulant
$M_{I_S}(s)$	Moment generating function of I_S
$f_h(h)$	PDF of random variable h
$Q(\cdot)$	Q-function
$\bar{F}_{I_{\text{total}}}(I)$	CCDF of total interference I_{total}
β_{target}	Target of outage probability
$\Gamma(\cdot)$	Gamma function
m_{N}	Nakagami-m fading parameter
$\sigma_{\text{S,dB}}$	Log-normal shadowing parameter
ξ	$10/\ln(10)$
$g(r,\theta,\varphi)$	Radar's antenna gain
G_{m}	Mainlobe gain
G_{s}	Sidelobe gain
θ_{d}	Mainlobe beamwidth

II. SYSTEM MODEL

A. SYSTEM OUTLINE

We consider UAV networks in 3D space $\mathbb{R}^2 \times \mathbb{R}^+$. Radar using the wide shared band is located at the origin and the UAVs are assumed to follow an *inhomogeneous* 3D PPP to present a stochastic geometry framework to design a 3D-shaped PER. The study introduces two types of spatial grids, namely cylindrical and cubic, to design the complex-shaped PER according to the primary user's antenna pattern.

B. CYLINDRICAL GRID

Fig. 1 displays an outline of the cylindrical grid. The grid divides the space into $M_r M_\theta M_z$ grid cells where M_r, M_θ, and M_z denote the number of radial, angular, and height divisions, respectively. We assume that all grid cells exhibit the same volume. Subsequently, each grid cell $U_{ijk} \subset \mathbb{R}^2 \times \mathbb{R}^+$ for $i \in \mathcal{I}_1 = \{0, 1, \ldots, M_r - 1\}, j \in \mathcal{J}_1 = \{0, 1, \ldots, M_\theta - 1\}$,

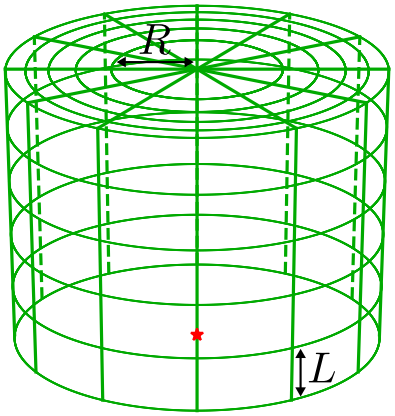

FIGURE 1. Cylindrical grid model.

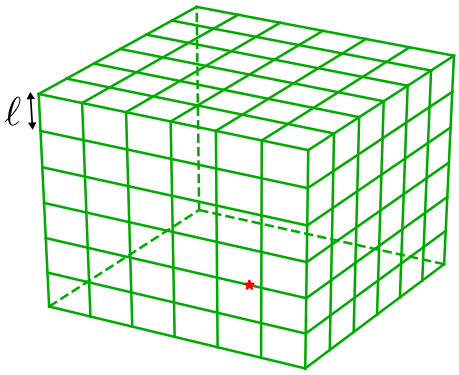

FIGURE 2. Cubic grid model.

and $k \in \mathcal{K}_1 = \{0, 1, \ldots, M_z - 1\}$, is expressed as follows:

$$U_{ijk} = \{(r, \theta, z) \mid R\sqrt{i} \le r < R\sqrt{i+1}, \\ 2\pi j/M_\theta \le \theta < 2\pi(j+1)/M_\theta, kL \le z < (k+1)L\}, \quad (1)$$

where R denotes the radius of U_{0jk} and L denotes the height of each grid cell. It should be noted that the volume of all grid cells correspond to $\pi R^2 L/M_\theta$. Evidently, $\{U_{ijk}\}_{i\in\mathcal{I}_1, j\in\mathcal{J}_1, k\in\mathcal{K}_1}$ are disjoint from each other. Moreover, we set these parameters such that the interference at the radar from UAVs outside $\bigcup_{i\in\mathcal{I}_1}\bigcup_{j\in\mathcal{J}_1}\bigcup_{k\in\mathcal{K}_1} U_{ijk}$ is negligible.

C. CUBIC GRID

Fig. 2 displays an outline of the cubic grid. The grid divides the space into $N_x N_y N_z$ grid cells, where N_x, N_y, and N_z denote the number of x-axis, y-axis, and z-axis divisions, respectively. Subsequently, each grid cell $V_{ijk} \subset \mathbb{R}^2 \times \mathbb{R}^+$ for $i \in \mathcal{I}_2 = \{0, 1, \ldots, N_x - 1\}, j \in \mathcal{J}_2 = \{0, 1, \ldots, N_y - 1\}$, and $k \in \mathcal{K}_2 = \{0, 1, \ldots, N_z - 1\}$ is expressed as follows:

$$V_{ijk} = \{(x, y, z) \mid i\ell \le x < (i+1)\ell, \\ j\ell \le y < (j+1)\ell, \ k\ell \le z < (k+1)\ell\}, \quad (2)$$

where ℓ denotes the length of a side of the cube. It should be noted that the volume of all grid cells correspond to ℓ^3.

D. DISTRIBUTION OF UAVS

This section focuses on a single grid cell S; S is U_{ijk} or V_{ijk} in the cylindrical or cubic grid models, respectively. Let the volume (Lebesgue measure) of S be denoted by $|S|$. With respect to each S, the density of UAVs is denoted as λ_S, and the constant gain generated from the antenna patterns of the radar is denoted as g_S. The UAVs are assumed to follow an inhomogeneous 3D PPP, not only on the surface of the grid cells. Let the inhomogeneous PPP and its intensity function be denoted by Φ_S and Λ_S, respectively. $\Lambda_S : \mathbb{R}^2 \times \mathbb{R}^+ \to \mathbb{R}$ is defined as

$$\Lambda_S(u) := \begin{cases} \lambda_S & \text{if } u \in S, \\ 0 & \text{otherwise.} \end{cases} \quad (3)$$

We introduce the UAV's ATP in S as a_S with $0 \le a_S \le 1$. UAVs with ratio a_S in S are allowed to transmit in the wide shared band; the others can only transmit in the narrow dedicated band. That is, $\{S : 0 < a_S < 1\}$ represents a PER where some, yet not all, UAVs are allowed to transmit in the wide shared band, and $\{S : a_S = 0\}$ represents a PER where no UAVs are allowed to transmit. Note that by introducing the ATP, we can design a PER as the solution of a continuous optimization problem [4].

The UAVs allowed to transmit in the wide shared band in S also follow an inhomogeneous PPP, and their intensity function is expressed as $a_S\Lambda_S(u)$. Let the inhomogeneous PPP be denoted as $\hat{\Phi}_S$.

III. OUTAGE PROBABILITY

The radar's OP is defined as the probability that the aggregate interference power I_{total} at the radar from all UAVs transmitting in the wide shared band exceeds the threshold I_{th}. Thus, the radar's OP is expressed as $\mathbb{P}(I_{\text{total}} > I_{\text{th}})$.

A. AGGREGATED INTERFERENCE

The aggregated interference I_{total} is defined as follows:

$$I_{\text{total}} = \sum_S I_S, \quad (4)$$

where I_S denotes the interference at the radar from the UAVs allowed to transmit in a single grid cell S, and I_S is expressed as follows:

$$I_S = \sum_{d\in\hat{\Phi}_S} g_S p_S h_d \|d\|^{-\alpha}, \quad (5)$$

where h_d denotes the fading gain that is randomly distributed with unit mean between $d \in \hat{\Phi}_S$ and the origin, p_S denotes the transmission power level of the UAVs in S, $\|d\|$ denotes the Euclidean distance between $d \in \mathbb{R}^3$ and the origin, and α denotes the path-loss exponent. We assume that the fading gain, h_d, is an independent and identically distributed (i.i.d.) random variable, h, with a probability density function (PDF), f_h.

B. INTERFERENCE CUMULANT

To derive the distribution of the interference, we calculate the nth cumulant of I_{total}. Let the nth cumulant of a random variable, X, for $n = 1, 2, \ldots$ be denoted by $\kappa_n(X)$. $\kappa_n(X)$ for $n = 1, 2, \ldots$ uniquely determines the distribution of X.

Using the PGFL for PPP [9], the moment generating function of I_S, M_{I_S}, is expressed as follows:

$$\begin{aligned} M_{I_S}(s) &= \mathbb{E}(\mathrm{e}^{sI_S}) \\ &= \mathbb{E}(\mathrm{e}^{s\sum_{d\in\hat{\Phi}_S} g_S p_S h_d \|d\|^{-\alpha}}) \\ &= \mathbb{E}\left(\prod_{d\in\hat{\Phi}_S} \mathrm{e}^{s g_S p_S h_d \|d\|^{-\alpha}}\right) \\ &= \exp\left[a_S\lambda_S \int_0^\infty\int_S (\mathrm{e}^{shg_S p_S\|d\|^{-\alpha}}-1) f_h(h)\,\mathrm{d}d\,\mathrm{d}h\right]. \end{aligned} \tag{6}$$

From (6), the nth cumulant of I_S, $\kappa_n(I_S)$, is obtained as

$$\begin{aligned} \kappa_n(I_S) &= \frac{\mathrm{d}^n}{\mathrm{d}s^n} \ln M_{I_S}(s)\Big|_{s=0} \\ &= a_S\lambda_S \int_S \mathbb{E}_h(g_S^n p_S^n \|d\|^{-n\alpha})\,\mathrm{d}d \\ &= a_S\lambda_S g_S^n p_S^n\, \mathbb{E}(h^n)\, A_n(S), \end{aligned} \tag{7}$$

$$\mathbb{E}(h^n) = \int_0^\infty h^n f_h(h)\,\mathrm{d}h, \tag{8}$$

$$A_n(S) = \int_S \|d\|^{-n\alpha}\,\mathrm{d}d. \tag{9}$$

We calculate $A_n(S)$ to obtain $\kappa_n(I_S)$ in cylindrical and cubic grid models in the following sections.

C. INTERFERENCE CUMULANT IN CYLINDRICAL GRID MODEL

In the cylindrical grid case, I_{total} is expressed as follows:

$$I_{\text{total}} = \sum_{k=0}^{M_z-1}\sum_{j=0}^{M_\theta-1}\sum_{i=0}^{M_r-1} I_{U_{ijk}}. \tag{10}$$

It should be noted that $\{I_{U_{ijk}}\}_{i\in\mathcal{I}_1, j\in\mathcal{J}_1, k\in\mathcal{K}_1}$ are mutually independent random variables because $\{\hat{\Phi}_{U_{ijk}}\}_{i\in\mathcal{I}_1, j\in\mathcal{J}_1, k\in\mathcal{K}_1}$ are mutually independent inhomogeneous PPPs. Thus, from the cumulant additivity property [14], $\kappa_n(I_{\text{total}})$ is expressed as follows:

$$\kappa_n(I_{\text{total}}) = \sum_{k=0}^{M_z-1}\sum_{j=0}^{M_\theta-1}\sum_{i=0}^{M_r-1} \kappa_n(I_{U_{ijk}}), \quad n = 1, 2, \ldots. \tag{11}$$

From (9), $A_n(U_{ijk})$ is calculated as follows:

$$\begin{aligned} &A_n(U_{ijk}) \\ &= \int_{z_k}^{z_{k+1}}\int_{\theta_j}^{\theta_{j+1}}\int_{r_i}^{r_{i+1}} r(r^2+z^2)^{-n\alpha/2}\,\mathrm{d}r\,\mathrm{d}\theta\,\mathrm{d}z \\ &= \left[\frac{2\pi(j+1)}{M_\theta} - \frac{2\pi j}{M_\theta}\right]\int_{z_k}^{z_{k+1}}\int_{r_i}^{r_{i+1}} r(r^2+z^2)^{-n\alpha/2}\,\mathrm{d}r\,\mathrm{d}z \\ &= \frac{2\pi}{M_\theta}\int_{z_k}^{z_{k+1}}\int_{r_i}^{r_{i+1}} r(r^2+z^2)^{-n\alpha/2}\,\mathrm{d}r\,\mathrm{d}z, \end{aligned} \tag{12, 13}$$

where $r_i := R\sqrt{i}$, $\theta_j := 2\pi j/M_\theta$, and $z_k := kL$. When α corresponds to an integer greater than two, the integral in (13) converges. In the specific case of $\alpha = 3$, $\kappa_1(I_{U_{ijk}})$ and $\kappa_2(I_{U_{ijk}})$ are calculated as in the following closed forms:

$$\begin{aligned} \kappa_1(I_{U_{ijk}}) &= a_{U_{ijk}}\lambda_{U_{ijk}} g_{U_{ijk}} p_{U_{ijk}}\, \mathbb{E}(h)\frac{2\pi}{M_\theta} \\ &\quad\cdot [b_1(r_i) - b_1(r_{i+1})], \end{aligned} \tag{14}$$

$$\begin{aligned} \kappa_2(I_{U_{ijk}}) &= a_{U_{ijk}}\lambda_{U_{ijk}} g_{U_{ijk}}^2 p_{U_{ijk}}^2\, \mathbb{E}(h^2)\frac{\pi}{4M_\theta} \\ &\quad\cdot [c_1(r_i) - c_1(r_{i+1})], \end{aligned} \tag{15}$$

$$b_1(r) = \ln\frac{z_{k+1} + \sqrt{r^2 + {z_{k+1}}^2}}{z_k + \sqrt{r^2 + z_k^2}}, \tag{16}$$

$$\begin{aligned} c_1(r) = {} & \frac{1}{r^3(r^2+z_k^2)(r^2+z_{k+1}^2)} \\ & \cdot\{[r^4 + r^2(z_k^2 + z_{k+1}^2) + z_k^2 z_{k+1}^2] \\ & \cdot[\arctan(z_{k+1}/r) - \arctan(z_k/r)] \\ & + r(r^2 - z_k z_{k+1})(z_{k+1} - z_k)\}. \end{aligned} \tag{17}$$

D. INTERFERENCE CUMULANT IN CUBIC GRID MODEL

In the cubic grid case, I_{total} is expressed as follows:

$$I_{\text{total}} = \sum_{k=0}^{N_z-1}\sum_{j=0}^{N_y-1}\sum_{i=0}^{N_x-1} I_{V_{ijk}}. \tag{18}$$

$\{I_{V_{ijk}}\}_{i\in\mathcal{I}_2, j\in\mathcal{J}_2, k\in\mathcal{K}_2}$ are mutually independent random variables because $\{\hat{\Phi}_{V_{ijk}}\}_{i\in\mathcal{I}_2, j\in\mathcal{J}_2, k\in\mathcal{K}_2}$ are mutually independent inhomogeneous PPPs. Thus, from the cumulant additivity property [14], $\kappa_n(I_{\text{total}})$ is expressed as follows:

$$\kappa_n(I_{\text{total}}) = \sum_{k=0}^{N_z-1}\sum_{j=0}^{N_y-1}\sum_{i=0}^{N_x-1} \kappa_n(I_{V_{ijk}}), \quad n = 1, 2, \ldots. \tag{19}$$

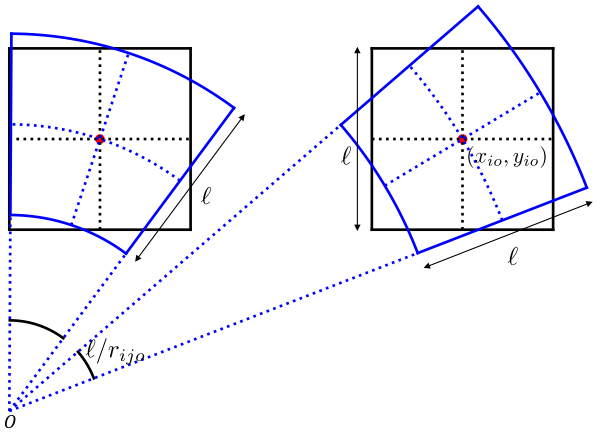

FIGURE 3. Top view of cubic grid cells (black) approximated by cylindrical grid cells (blue).

In this case, it is not possible to express $A_n(V_{ijk})$ in (9) in a closed-form expression because the volume integral in (9) cannot be expressed in a closed form. We approximate V_{ijk} by a cylindrical grid cell as in Fig. 3 to obtain $A_n(V_{ijk})$ in a closed

form. The grid cells exhibit the same volume and satisfy the following conditions:

1) The grid cells exhibit the same length in the z-axis.
2) The point of intersection of the midpoint of the radial side and midpoint of the circumference are equal to the point of intersection of the diagonals of the square grid cell. The coordinates of the point are expressed as $(x_{io}, y_{jo}) := (\frac{2i+1}{2}\ell, \frac{2j+1}{2}\ell)$ in the Cartesian coordinates and $(r_{ijo}, \theta_{ijo}) := \left((x_{io}^2 + y_{jo}^2)^{1/2}, \arctan\frac{2j+1}{2i+1}\right)$ in the polar coordinates.
3) The radial length of the approximated grid cell is ℓ.
4) The central angle of the approximated grid cell is ℓ/r_{ijo}.

Subsequently, $A_n(V_{ijk})$ is approximated as follows:

$$\begin{aligned} &A_n(V_{ijk}) \\ &\approx \int_{k\ell}^{(k+1)\ell}\int_{\theta_{ijo}-\ell/2}^{\theta_{ijo}+\ell/2}\int_{r_{ijo}}^{r_{ijo}+\ell/2} (r^2+z^2)^{-n\alpha/2}\, r\,\mathrm{d}r\,\mathrm{d}\theta\,\mathrm{d}z \\ &= \frac{\ell}{r_{ijo}}\int_{k\ell}^{(k+1)\ell}\int_{r_{ijo}-\ell/2}^{r_{ijo}+\ell/2} r(r^2+z^2)^{-n\alpha/2}\,\mathrm{d}r\,\mathrm{d}z. \end{aligned} \tag{20}$$

The validity of the approximation is established via numerical evaluations in Section V. When α corresponds to an integer greater than two, the integral in (20) converges. In the specific case of $\alpha = 3$, $\kappa_1(I_{V_{ijk}})$ and $\kappa_2(I_{V_{ijk}})$ are calculated in the following closed forms:

$$\begin{aligned} \kappa_1(I_{V_{ijk}}) =\ & a_{V_{ijk}}\lambda_{V_{ijk}} g_{V_{ijk}} p_{V_{ijk}}\, \mathbb{E}(h)\frac{\ell}{r_{ijo}} \\ & \cdot\left[b_2\big(r_{ijo}-\ell/2\big) - b_2\big(r_{ijo}+\ell/2\big)\right], \end{aligned} \tag{21}$$

$$\begin{aligned} \kappa_2(I_{V_{ijk}}) =\ & a_{V_{ijk}}\lambda_{V_{ijk}} g_{V_{ijk}}^2 p_{V_{ijk}}^2\, \mathbb{E}(h^2)\frac{\ell}{8r_{ijo}} \\ & \cdot\left[c_2\big(r_{ijo}-\ell/2\big) - c_2\big(r_{ijo}+\ell/2\big)\right], \end{aligned} \tag{22}$$

$$b_2(r) = \ln\left(\frac{(k+1)\ell+\sqrt{r^2+(k+1)^2\ell^2}}{k\ell+\sqrt{r^2+(k\ell)^2}}\right), \tag{23}$$

$$\begin{aligned} c_2(r) =\ & \frac{1}{r^3[r^2+(k\ell)^2][r^2+(k+1)^2\ell^2]}\{(r^4 \\ & + r^2[(k\ell)^2+(k+1)^2\ell^2] + (k\ell)^2(k+1)^2\ell^2) \\ & \times[\arctan((k+1)\ell/r) - \arctan(k\ell/r)] \\ & + r[r^2 - k\ell(k+1)\ell][(k+1)\ell - k\ell]\}. \end{aligned} \tag{24}$$

E. RADAR'S OUTAGE PROBABILITY

We use the cumulant matching approach [15], and the distribution of I_{total} is expressed approximately as a log-normal distribution [16]. Using (11) or (19), the PDF of I_{total}, $f_{I_{\text{total}}}$, is expressed approximately as follows:

$$f_{I_{\text{total}}}(I) \simeq \frac{1}{\sqrt{2\pi}\sigma_1\, I}\exp\left[-\frac{(\ln I-\mu_1)^2}{2{\sigma_1}^2}\right], \tag{25}$$

$$\mu_1 = \ln\left(\frac{\kappa_1(I_{\text{total}})^2}{\sqrt{\kappa_1(I_{\text{total}})^2+\kappa_2(I_{\text{total}})}}\right), \tag{26}$$

$${\sigma_1}^2 = \ln\left(\frac{\kappa_2(I_{\text{total}})}{\kappa_1(I_{\text{total}})^2}+1\right). \tag{27}$$

In this case, the complementary cumulative distribution function (CCDF) of I_{total} is expressed as follows:

$$\begin{aligned} \bar{F}_{I_{\text{total}}}(I) :=\ & \mathbb{P}(I_{\text{total}} > I) \\ \simeq\ & Q\left(\frac{\ln I-\mu_1}{\sigma_1}\right), \end{aligned} \tag{28}$$

where $Q(\cdot)$ denotes the Q-function, which is defined as $Q(x) = (1/\sqrt{2\pi})\int_x^\infty \exp(-t^2/2)\,\mathrm{d}t$. Note that the radar's OP for the specific threshold I_{th} is expressed using the CCDF as $\bar{F}_{I_{\text{total}}}(I_{\text{th}}) = \mathbb{P}(I_{\text{total}} > I_{\text{th}})$. Here, we consider I a variable and I_{th} a constant.

IV. OPTIMIZATION PROBLEM FOR DESIGNING PER

With the derived interference cumulants and CCDF, we determine a PER via an optimization problem. We define the objective function as the number of UAVs forbidden from transmitting signals and design an optimization problem to minimize this function. Furthermore, to ensure that UAV communications do not cause harmful interference with the radar, we impose the constraint that the radar's OP, $\bar{F}_{I_{\text{total}}}(I_{\text{th}})$, must be less than or equal to a target β_{target} as in [4].

A. CYLINDRICAL GRID

In the cylindrical grid model, we formulate the optimization problem as follows:

$$\begin{aligned} &\underset{(a_{U_{ijk}})_{i\in\mathcal{I}_1, j\in\mathcal{J}_1, k\in\mathcal{K}_1}}{\text{minimize}} \sum_{i\in\mathcal{I}_1}\sum_{j\in\mathcal{J}_1}\sum_{k\in\mathcal{K}_1}(1-a_{U_{ijk}})\lambda_{U_{ijk}}|U_{ijk}|, \\ &\text{subject to } \bar{F}_{I_{\text{total}}}(I_{\text{th}}) \le \beta_{\text{target}}, \\ &\qquad a_{U_{ijk}} \in [0,1]. \end{aligned} \tag{29}$$

This is a constrained nonlinear optimization problem. Note that (29) is equivalent to the problem of minimizing the volume of the PER when $\lambda_{U_{ijk}}$ is identical for all U_{ijk}.

B. CUBIC GRID

In the cubic grid model, we formulate the optimization problem as follows:

$$\begin{aligned} &\underset{(a_{V_{ijk}})_{i\in\mathcal{I}_2, j\in\mathcal{J}_2, k\in\mathcal{K}_2}}{\text{minimize}} \sum_{i\in\mathcal{I}_2}\sum_{j\in\mathcal{J}_2}\sum_{k\in\mathcal{K}_2}(1-a_{V_{ijk}})\lambda_{V_{ijk}}|V_{ijk}|, \\ &\text{subject to } \bar{F}_{I_{\text{total}}}(I_{\text{th}}) \le \beta_{\text{target}}, \\ &\qquad a_{V_{ijk}} \in [0,1]. \end{aligned} \tag{30}$$

V. NUMERICAL EVALUATION

We determine the optimized PER by solving (29) and (30). Subsequently, we calculate the CCDF of the aggregate interference in both grid cases via Monte Carlo simulations to evaluate the validity of the analytical results. Moreover, the number of UAVs transmitting in the wide shared band are evaluated.

For comparison, we assume that each grid cell in the cylindrical and cubic models exhibit the same volume. Subsequently, the side length of the cubic grid cell, ℓ, is expressed

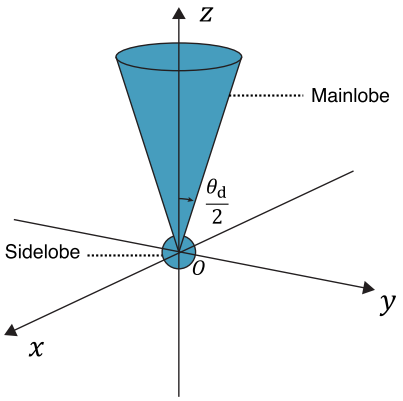

FIGURE 4. Keyhole antenna model.

as follows:

$$\ell = R\left(\frac{M_\theta}{\pi L}\right)^3. \tag{31}$$

We use Nakagami-m fading superimposed on log-normal shadowing [17], and thus $\mathbb{E}(h^n)$ is expressed as follows:

$$\mathbb{E}(h^n) = \frac{\Gamma(m_{\mathrm{N}}+n)}{\Gamma(m_{\mathrm{N}})\, {m_{\mathrm{N}}}^n} \exp\left[\frac{n(n-1){\sigma_{\mathrm{S,dB}}}^2}{2\xi^2}\right], \tag{32}$$

where $\Gamma(\cdot)$, m_{N}, and $\sigma_{\mathrm{S,dB}}$ denote the gamma function, Nakagami-m fading parameter, and log-normal shadowing parameter with a dB spread, respectively; $\xi = 10/\ln(10)$.

A. PARAMETERS

To ensure radar safety, we assume that the radar's antenna gain for each grid cell S, g_S, denotes the maximum value in S. Subsequently, g_S is generated as follows:

$$g_S = \max_{(r,\theta,\varphi)\in S} g(r,\theta,\varphi),$$

where $g(r,\theta,\varphi)$ denotes the radar's antenna gain. As indicated in Fig. 4, $g(r,\theta,\varphi)$ is assumed to be a keyhole antenna model [18] consisting of a mainlobe with bandwidths θ_{d} and sidelobes for other directions. $g(r,\theta,\varphi)$ is expressed as follows:

$$g(r,\theta,\varphi) = \begin{cases} G_{\mathrm{m}} & \text{if } 0 \le \theta \le \theta_{\mathrm{d}}/2, \\ G_{\mathrm{s}} & \text{otherwise}, \end{cases} \tag{33}$$

where G_{m} and G_{s} denote the gains of the mainlobe and sidelobe, respectively. G_{m} and G_{s} satisfy the following equation:

$$G_{\mathrm{s}} = \frac{2 - G_{\mathrm{m}}[1-\cos(\theta_{\mathrm{d}}/2)]}{1+\cos(\theta_{\mathrm{d}}/2)}. \tag{34}$$

We use the Pyomo modeling framework [19] to formulate (29) and (30) and solve the continuous nonlinear optimization problem numerically via the Interior Point Optimizer (IPOPT) solver [20] for continuous nonlinear optimization problems.

For simplicity, the density of UAVs, λ_S, and transmission power of the UAVs, p_S, in each grid cell are assumed to be identical. Table 2 displays the parameter values.

TABLE 2. Parameters.

Parameter	Value
α	3
G_{m}	14
θ_{d}	$\pi/6$
p_S	1 W
λ_S	$6.25 \times 10^{-7}\ \mathrm{m}^{-3}$
m_{N}	1
$\sigma_{\mathrm{S,dB}}$	6
I_{th}	6.0×10^{-7} W
β_{target}	10^{-2}

B. NUMERICAL RESULTS

Figs. 5 and 6 display the radar's antenna gain and corresponding optimized PER in a 2D manner for each height in the cylindrical and cubic grid models, respectively. As indicated in these figures, the PER is designed according to the radar's antenna pattern. Moreover, a large PER is realized in the direction with high antenna gain and a small PER is realized in the direction with low antenna gain.

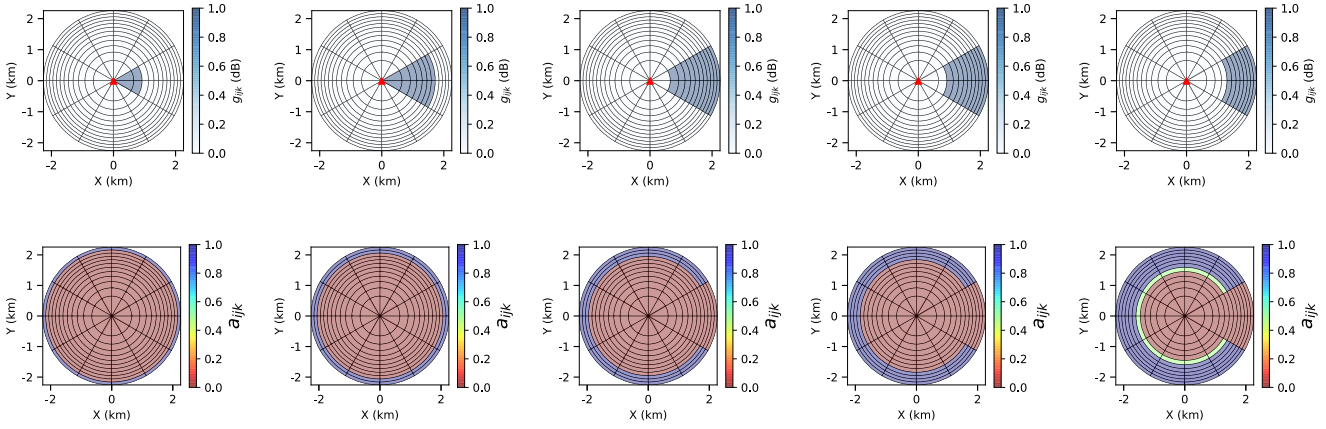

(a) 0–0.33 km. (b) 0.33–0.67 km. (c) 0.67–1.0 km. (d) 1.0–1.33 km. (e) 1.33–1.67 km.

FIGURE 5. Radar's antenna gain (upper) and optimized PER (lower) according to radar's antenna pattern in cylindrical grid case when volume of grid cells corresponds to 0.33^3 km^3. Blue grid cells in antenna gains include mainlobe and red grid cells in optimized PERs denote the PER.

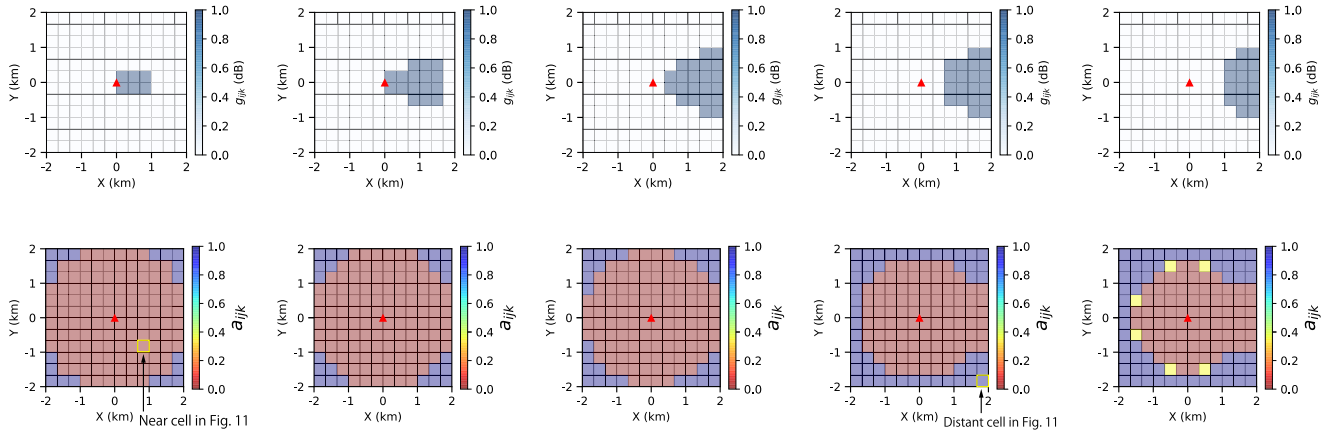

(a) 0–0.33 km. (b) 0.33–0.67 km. (c) 0.67–1.0 km. (d) 1.0–1.33 km. (e) 1.33–1.67 km.

FIGURE 6. Radar's antenna gain (upper) and optimized PER (lower) according to radar's antenna pattern in cubic grid case when volume of grid cells corresponds to 0.33^3 km^3. Blue grid cells in antenna gains include mainlobe and red grid cells in the optimized PERs denote the PER.

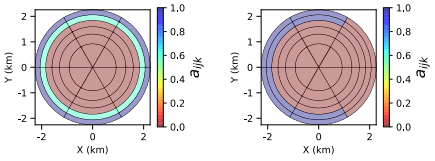

(a) 0–0.67 km. (b) 0.67–1.33 km.

FIGURE 7. Optimized PER in each height in cylindrical grid case when volume of grid cells corresponds to 0.67^3 km^3.

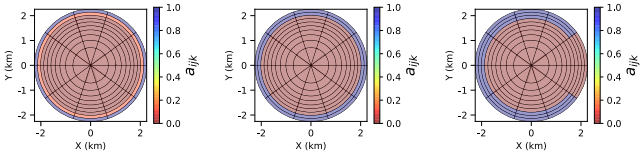

(a) 0–0.5 km. (b) 0.5–1.0 km. (c) 1.0–1.5 km.

FIGURE 8. Optimized PER in each height in cylindrical grid case when volume of grid cells corresponds to 0.4^3 km^3.

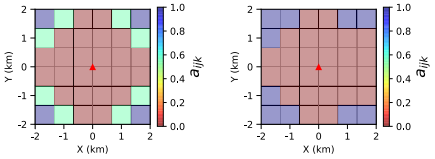

(a) 0–0.67 km. (b) 0.67–1.33 km.

FIGURE 9. Optimized PER in each height in cubic grid case when volume of grid cells corresponds to 0.67^3 km^3.

Figs. 7 and 8 compare the optimized PER when the volume of the grid cells varies in the cylindrical grid case. Figs. 9 and 10 compare the optimized PER when the volume of the grid cells varies in the cubic grid case. As indicated in the figures, decreases in the volume of the grid cell cause the designed PER to shrink and become complex-shaped in both grid cases.

A complex-shaped PER is an advantage of the proposed framework compared to a conventional upper-hemisphere

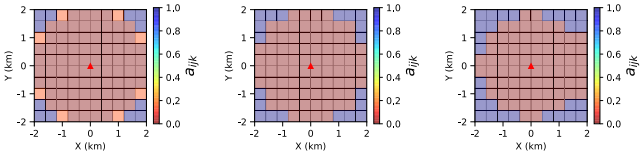

(a) 0–0.4 km. (b) 0.4–0.8 km. (c) 0.8–1.2 km.

FIGURE 10. Optimized PER in each height in cubic grid case when volume of grid cells corresponds to 0.4^3 km^3.

PER [6], [7] where the radius of the PER is the only parameter that must be determined based on the mainlobe gain. That is, the radius of a conventional upper-hemisphere PER can be calculated as the maximum distance between the origin and grid cells where the ATP is zero. Thus, the conventional PER design overestimates the interference and excessively prohibits the transmissions of UAVs, especially towards the sidelobe of the radar.

To validate the approximation (20), we evaluated the empirical cumulative distribution function (ECDF) of the interference power from representative grid cells via the Monte Carlo simulation. Fig. 11 displays the ECDF of the interference power from the UAVs in the cubic grid cells and its approximated grid cells. The results indicate that the difference of the ECDF is small, and thus the approximation is valid. However, the difference of the ECDF of a distant grid cell is greater than that of a near grid cell because the volume of overlap between the two grid cells of the distant grid cell is less than that of a near grid cell.

Fig. 12 displays the CCDF of I_{total}, $\bar{F}_{I_{\text{total}}}(I)$, in the cylindrical and cubic grid cases. The broken lines are obtained via a Monte Carlo simulation with 10^4 runs and the solid lines are obtained by (28). The numerical evaluation of (28) confirms that the constraints of the problems (29) and (30) are satisfied, where $\beta_{\text{target}} = 10^{-2}$ and $I_{\text{th}} = 6.0 \times 10^{-7}$ W $= -32.2$ dBm. Furthermore, the simulation result is in acceptable agreement with the theoretical result in the cylindrical grid case. However, a difference exists between the simulation results

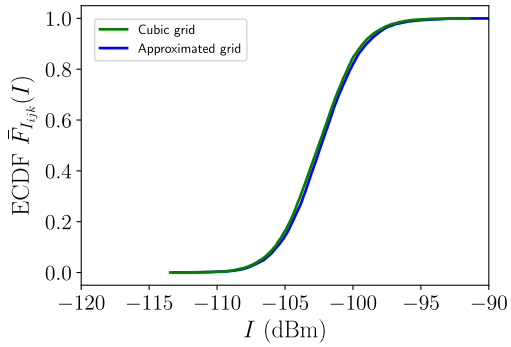

(a) From near grid cell ($0.67 \leq x \leq 1$, $-1 \leq y \leq -0.67$, $0 \leq z \leq 0.33$) in Fig. 6 (a).

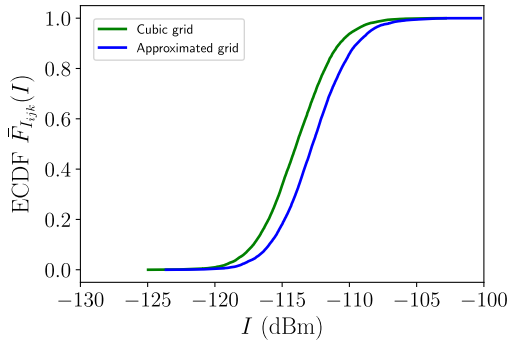

(b) From distant grid cell ($1.67 \leq x \leq 2$, $-2 \leq y \leq -1.67$, $1 \leq z \leq 1.33$) in Fig. 6 (d).

FIGURE 11. ECDF of interference power at radar when volume of grid cells corresponds to 0.33^3 km^3.

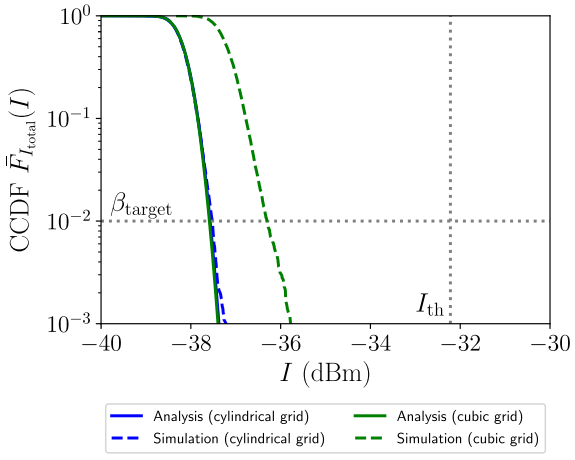

FIGURE 12. CCDF of aggregate interference I_{total}, $\bar{F}_{I_{\text{total}}}(I)$, when volume of grid cells corresponds to 0.33^3 km^3. Two curves, "Analysis (cylindrical grid)" and "Analysis (cubic grid)" are overlapped. Radar's OP, $F_{I_{\text{total}}}(I_{\text{th}})$, satisfies β_{target} for all curves.

and theoretical result in the cubic grid case. This is because we assume the worst case with respect to antenna gain. A large difference exists between g_S and $g(r, \theta, \varphi)$ in the cubic grid case.

Fig. 13 displays the number of UAVs transmitting in the wide shared band, $\sum_S a_S \lambda_S |S|$, for each spatial grid. In the cylindrical grid case, we use the following

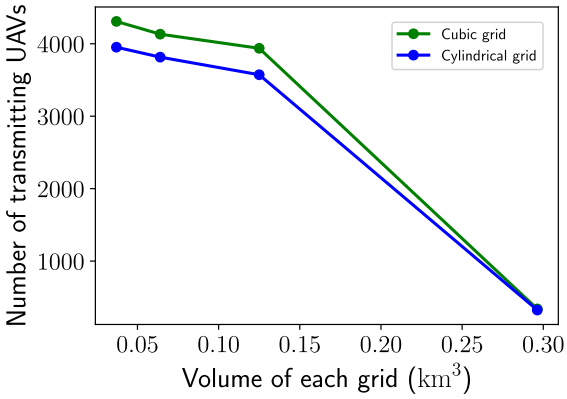

FIGURE 13. Number of UAVs transmitting in wide shared band in the cylindrical and cubic grid cases.

parameters, $(M_r, M_\theta, M_z, L) = (12, 12, 5, 1000/3)$, $(10, 10, 4, 400)$, $(8, 8, 3, 500)$, $(6, 6, 2, 2000/3)$, $N_x = N_y = M_r$, and $N_z = M_z$. R is calculated using (31) by setting $\ell = L$. The number of UAVs transmitting in the wide shared band increases with decreases in the volume of each grid cell. Moreover, the number of UAVs transmitting in the wide shared band in the cubic grid case exceeds that of the cylindrical grid case. This is because in the cylindrical grid case, the interference is overestimated, unlike in the cubic grid case. Specifically, interference from grid cells partially towards the mainlobe is estimated as interference totally towards the mainlobe to ensure radar safety.

VI. CONCLUSION

This study presented a stochastic geometry analysis of interference in UAV networks and proposed a design for an optimal PER based on cylindrical and cubic grid models. The transmission probability of the transmitting UAVs for each grid cell was determined from the PER. The radar's OP was analytically derived by considering the UAV distribution in each grid cell as an inhomogeneous PPP. The derived expression was used, and the optimization problem was formulated. This maximizes the number of UAVs using the wide shared band under the constraint of the radar's OP target. Subsequently, the solution of the optimization problem was numerically evaluated. The results indicate that the PER is designed according to the radar's antenna pattern and that the number of transmitting UAVs increases with increases in the number of divisions.

ACKNOWLEDGMENT

This paper was presented in part at the IEEE Consumer Communications and Networking Conference (CCNC) 2019.

REFERENCES

[1] The Information and Communications Council. (Jan. 2016) *Technical Requirements for Upgrading of use of Radio Waves for Robots, etc.* (in Japanese). [Online]. Available: http://www.soumu.go.jp/main_content/000397220.pdf

[2] M. Vu, N. Devroye, and V. Tarokh, "On the primary exclusive region of cognitive networks," *IEEE Trans. Wireless Commun.*, vol. 8, no. 7, pp. 3380–3385, Jul. 2009.

[3] S. Yamashita, K. Yamamoto, T. Nishio, and M. Morikura, "Knowledge-based reestablishment of primary exclusive region in database-driven spectrum sharing" *IEICE Trans. Commun.*, vol. 99, no. 9, pp. 2019–2027, Sep. 2016.
[4] S. Yamashita, K. Yamamoto, T. Nishio, and M. Morikura, "Exclusive region design for spatial grid-based spectrum database: A stochastic geometry approach," *IEEE Access*, vol. 6, pp. 24443–24451, 2018.
[5] J. Carle, J.-F. Myoupo, and D. Seme, "A basis for 3-D cellular networks," in *Proc. 15th Int. Conf. Inf. Netw.*, Beppu, Japan, Jan./Feb. 2001, pp. 631–636.
[6] C. Zhang and W. Zhang, "Spectrum sharing for drone networks," *IEEE J. Sel. Areas Commun.*, vol. 35, no. 1, pp. 136–144, Jan. 2016.
[7] K. Yoshikawa, S. Yamashita, K. Yamamoto, T. Nishio, and M. Morikura, "Resource allocation for 3D drone networks sharing spectrum bands," in *Proc. IEEE 86th Veh. Tech. Conf. (VTC-Fall)*. Toront, Canada, Sep. 2017, pp. 1–5.
[8] K. Yoshikawa, K. Yamamoto, T. Nishio, and M. Morikura, "Grid-based design for the 3D primary exclusive region in uav networks," in *Proc. 16th IEEE Annu. Consum. Commun. Netw. Conf. (CCNC)*. Las Vegas, USA, Jan. 2019, pp. 1–5.
[9] M. Haenggi, *Stochastic Geometry for Wireless Networks*. Cambridge, U.K.: Cambridge Univ. Press, 2012.
[10] H. ElSawy, E. Hossain, and M. Haenggi, "Stochastic geometry for modeling, analysis, and design of multi-tier and cognitive cellular wireless networks: A survey," *IEEE Commun. Surveys Tuts.*, vol. 15, no. 3, pp. 996–1019, 3rd Quart., 2013.
[11] X. Lin, J. G. Andrews, and A. Ghosh, "Spectrum sharing for device-to-device communication in cellular networks," *IEEE Trans. Commun.*, vol. 13, no. 12, pp. 6727–6740, Dec. 2014.
[12] F. Paisana, N. Marchetti, and L. A. DaSilva, "Radar, TV and cellular bands: Which spectrum access techniques for which bands?" *IEEE Commun. Surveys Tuts.*, vol. 16, no. 3, pp. 1193–1220, 3rd Quart., 2014.
[13] K. Sato, M. Kitamura, K. Inage, and T. Fujii, "Measurement-based spectrum database for flexible spectrum management," *IEICE Trans. Commun.*, vols. E98–B, no. 10, pp. 2004–2013, Oct. 2015.
[14] J. F. Kenney and E. S. Keeping, *Mathematics of Statistics part II*, 3rd ed. Princeton, NJ, USA: Van Nostrand, 1957.
[15] D. Schleher, " Generalized Gram-Charlier series with application to the sum of log-normal variates (Corresp.)," *IEEE Trans. Inf. Theory*, vol. IT-23, no. 2, pp. 275–280, May 1977.
[16] K. W. Sung, M. Tercero, and J. Zander, "Aggregate interference in secondary access with interference protection," *IEEE Commun. Lett.*, vol. 15, no. 6, pp. 629–631, Jun. 2011.
[17] M. K. Simon and M.-S. Alouini, *Digital Communication over Fading Channels*. Hoboken, NJ, USA: Wiley, 2004.
[18] P. Li, C. Zhang, and Y. Fang, "The capacity of wireless ad hoc networks using directional antennas," *IEEE Trans. Mobile Comput.*, vol. 10, no. 10, pp. 1374–1387, Oct. 2011.
[19] W. E. Hart, C. Laird, J.-P. Watson, and D. L. Woodruff, *Pyomo—Optimization Modeling in Python*, vol. 67. New York, NY, USA: Springer, 2012.
[20] A. Wächter and L. T. Biegler, "On the implementation of an interior-point filter line-search algorithm for large-scale nonlinear programming," *Math. Program.*, vol. 106, no. 1, pp. 25–27, Mar. 2006.

KEIJI YOSHIKAWA received the B.E. degree in electrical and electronic engineering from Kyoto University, in 2017, where he is currently pursuing the M.I. degree with the Graduate School of Informatics.

KOJI YAMAMOTO received the B.E. degree in electrical and electronic engineering and the M.E. and Ph.D. degrees in informatics from Kyoto University, in 2002, 2004, and 2005, respectively.

From 2004 to 2005, he was a Research Fellow with the Japan Society for the Promotion of Science (JSPS). Since 2005, he has been with the Graduate School of Informatics, Kyoto University, where he is currently an Associate Professor. From 2008 to 2009, he was a Visiting Researcher with Wireless@KTH, Royal Institute of Technology (KTH), Sweden. He has been an Editor of the IEEE WIRELESS COMMUNICATIONS LETTERS, since 2017, and the Track Co-Chairs of APCC 2017 and CCNC 2018. His research interests include radio resource management and applications of game theory.

Dr. Yamamoto received the PIMRC 2004 Best Student Paper Award, in 2004, the Ericsson Young Scientist Award, in 2006. He also received the Young Researcher's Award, the Paper Award, SUEMATSU-Yasuharu Award from the IEICE of Japan, in 2008, 2011, and 2016, respectively, and the IEEE Kansai Section GOLD Award, in 2012.

TAKAYUKI NISHIO received the B.E. degree in electrical and electronic engineering from Kyoto University, Kyoto, Japan, in 2010. He received the M.I. and Ph.D. degrees in communications and computer engineering from the Graduate School of Informatics, Kyoto University, in 2012 and 2013, respectively.

From 2012 to 2013, he was a Research Fellow (DC1) of the Japan Society for the Promotion of Science (JSPS). Since 2013, he has been an Assistant Professor in communications and computer engineering with the Graduate School of Informatics, Kyoto University. From 2016 to 2017, he was a Visiting Researcher with the Wireless Information Network Laboratory (WINLAB), Rutgers University, USA. His current research interests include mmwave networks, wireless local area networks, application of machine learning, and sensor fusion in wireless communications. He received the IEEE Kansai Section Student Award, in 2011, the Young Researcher's Award from the IEICE of Japan, in 2016, and the Funai Information Technology Award for Young Researchers, in 2016. He is a member of ACM and IEICE.

MASAHIRO MORIKURA received the B.E., M.E., and Ph.D. degrees in electronic engineering from Kyoto University, Kyoto, Japan, in 1979, 1981, and 1991, respectively. He joined NTT, in 1981, where he was involved in the research and development of TDMA equipment for satellite communications. From 1988 to 1989, he was with the Communications Research Centre, Canada, as a Guest Scientist. From 1997 to 2002, he was active in standardization of the IEEE802.11a-based wireless LAN. He is currently a Professor with the Graduate School of Informatics, Kyoto University. He received Paper Award and Achievement Award from the IEICE, in 2000 and 2006, respectively. He also received Education, Culture, Sports, Science, and Technology Minister Award, in 2007, and the Medal of Honor with Purple Ribbon from Japan's Cabinet Office, in 2015. He is a Fellow of the IEICE.